

Computational fluid dynamics simulation for tuned liquid column dampers in horizontal motion

Cheng-Hsin Chang*

*Department of Civil Engineering and Wind Engineering Research Center
Tamkang University, Tamsui, Taipei County, Taiwan*

(Received December 18, 2009, Accepted April 6, 2011)

Abstract. A Computational Fluid Dynamics model is presented in this study for the simulation of the complex fluid flows with free surfaces inside the Tuned Liquid Column Dampers in horizontal motion. The characteristics of the fluid model of the TLCD in horizontal motion include the free surface of the multiphase flow and the horizontal moving frame. In this study, the time depend unsteady Standard $k-\varepsilon$ turbulent model based on Navier-Stokes equations is chosen. The volume of fluid (VOF) method and sliding mesh technique are adopted to track the free surface of water inside the vertical columns of TLCD and treat the moving boundary of the walls of TLCD in horizontal motion. Several model solution parameters comprising different time steps, mesh sizes, convergence criteria and discretization schemes are examined to establish model parametric independency results. The simulation results are compared with the experimental data in the dimensionless amplitude of the water column in four different configured groups of TLCDs with four different orifice areas. The predicted natural frequencies and the head loss coefficient of TLCDs from CFD model are also compared with the experimental data. The predicted numerical results agree well with the available experimental data.

Keywords: CFD; TLCD; VOF; sliding mesh.

1. Introduction

In recent years, the newly developed construction technologies toward lighter and stronger materials have facilitated the realization of more and more high-rise buildings in many urban areas where space usage is demanding. The typical examples are the Petronas Twin Tower (452 m) in Kuala Lumpur, Malaysia, and Taipei 101 Building (508 m) in Taipei, Taiwan and the under-construction super-high building – Burj Dubai (807.7 m) in Dubai. However, the down side with it is the high susceptibility of their responses to wind loading, especially the induced acceleration magnification frequently causes occupants' discomfort. Thus, for structures such as these, it is very desirable to use control devices for the sake of vibration suppression. Among many varieties of control devices, the tuned liquid column damper (termed as TLCD) that is composed of fluid in a U-shape of liquid column container is a good candidate. During a motion, this device can dissipate energy by the relative movement of the fluid passing through an orifice located in the liquid column. In terms of advantages over other types of energy-dissipating dampers, the properties of

* Corresponding Author, Associate Professor, E-mail: cc527330@mail.tku.edu.tw

TLCD (such as the natural frequency and damping) can be reliably and precisely determined from the length of the liquid column and the orifice size.

The original idea of TLCD was developed by Sakai *et al.* (1989) for suppression of horizontal motion of structures. After that, quite a few research papers, namely Xu *et al.* (1992), Hitchcock *et al.* (1997), Balendra *et al.* (1998), and Felix *et al.* (2005) have verified its effectiveness for suppressing wind-induced horizontal responses, among whom Hitchcock *et al.* even investigated a general type of TLCDs that have non-uniform cross-sections in the horizontal and vertical columns, termed as liquid column vibration absorber (LCVA). De Souza *et al.* (2006) examined the effect of a liquid damper in some dynamical regimes characterized by coexistence of both periodic and chaotic motion. Chen and Ding (2008) investigated the dynamic characteristics of the passive, semi-active, and active TLCDs. Recently, the application of TLCDs was further extended to the suppression of pitching motion for bridge decks (e.g., Xue *et al.* (2000) and Wu *et al.* (2008)). For the application to the control of horizontal motion toward implementation, some researchers have spent efforts on determining optimal TLCD designs, such as Chang (1999) on undamped structures, Wu *et al.* (2005) on damped structures, and Yalla *et al.* (2000) on both damped and undamped structures. Some researchers focused on different type of TLCD. Fu (2009) investigated the influence of several tuned liquid column gas damper (TLCGD) with gas-spring effect to reduce coupled translational and rotational vibrations of plan-asymmetric buildings under wind or seismic loads.

Computational fluid dynamics (CFD) is one of the branches of fluid mechanics that uses numerical methods and algorithms to solve and analyze problems that involve fluid flows. The advanced technology makes computers faster and more powerful, which allows CFD procedures to be applied to many experimental flow problems. Today, increasing applications of CFD to engineering problems include wind, marine, chemical, and hydraulic engineering. Adding functions of the Volume of Fluid (VOF) and sliding mesh, the free surface and moving computing domain problems can be solved by CFD. Liovic *et al.* (2001) used the VOF approach for tracking the interface distortions of flow. Martinez-Calle *et al.* (2002) applied the sliding mesh technique to account for the rotation in an open water numerical model for marine propeller. Maronnier *et al.* (2003) solved the velocity field of three-dimensional free surface flows by VOF method. Chen *et al.* (2004) successfully simulated the turbulent flow field of the stepped spillway by $k-\varepsilon$ turbulent and VOF model. Fixed and sliding meshed with unsteady Reynolds averaged Navier-Stokes equations had been used to simulate the aerodynamic characteristics of a rotating cylinder for the assessment of accuracy of rotating meshes by Filippon (2005). Recently, the VOF and sliding mesh models were combined to deal one problem. Chen *et al.* (2006) employed both the sliding mesh and VOF models to simulate the flow in the surface flow accelerator system. Zhou *et al.* (2007) adopted the VOF method and sliding mesh technique to track the interface evolution and treat the moving boundaries of rotors during early stage of mixing of two immiscible polymer melts.

In this paper, CFD is used to simulate the water flow inside the TLCD in horizontal motion. The simulation results are compared to experimental measurements to predict the dimensionless amplitude of water column in the different configured groups of the TLCD. In the past, the information of the basic properties of the TLCD can be obtained only by performing the experiments. However, the costs and time of doing the physical experiments are usually very high. If a reliable computational fluid dynamic model can be developed to predict the information, it is beneficial for the structure engineers and the TLCD designers. With less time and money, the CFD simulation is helpful in getting the same result as the experiment without being restricted by space problems, for example, it is difficult to find a suitable place if a large size of the TLCD model is

needed. Moreover, a reliable CFD simulation usually can predict the experimental frame of the TLCD in advance of the experiment.

2. Experimental calibration of the TLCD properties

In order to provide more information on the basic properties of TLCDs, such as natural frequency and the head loss coefficient, this section presents the calibration results of TLCD properties in the free vibration and harmonic forced vibration tests using the shake table. A schematic diagram of a SDOF structure equipped with a TLCD under wind excitation is shown in Fig. 1. Four differently configured groups of TLCDs with uniform cross-sections as shown in Fig. 2 were constructed. The design of a rectangular cross-section and sharp-edged elbows is due to the simplicity in manufacturing. To examine if the size of liquid mass has effects on the basic properties, each configured group contains three TLCDs that each has the cross-section areas of $15\text{ cm} \times 15\text{ cm}$, $30\text{ cm} \times 15\text{ cm}$ and $45\text{ cm} \times 15\text{ cm}$, respectively. Since the damping of the TLCD is mainly

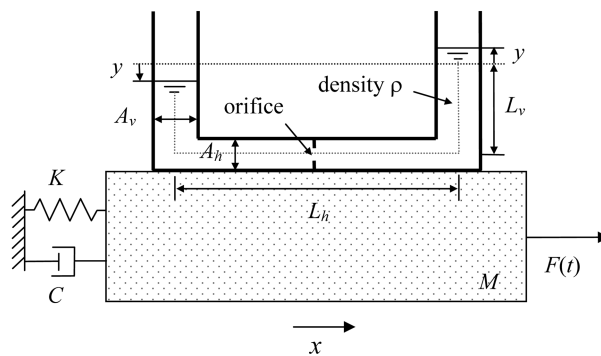


Fig. 1 SDOF Damped structure equipped with the TLCD under wind load

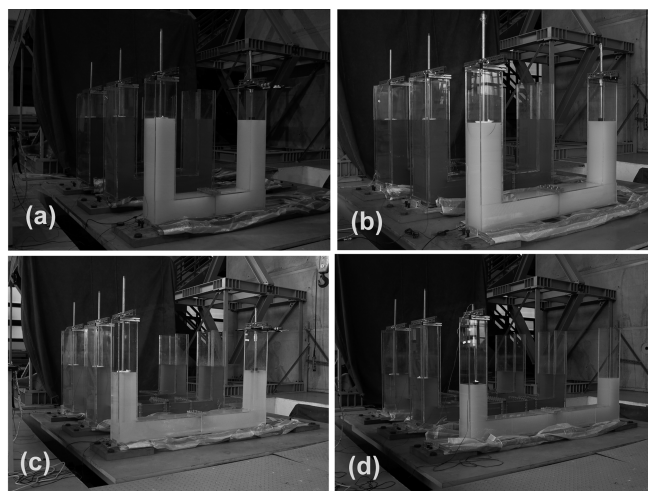


Fig. 2 Four configured groups of the TLCDs on the shake table: (a) configured group I, (b) configured Group II, (c) configured group III and (d) configured group IV

produced by energy dissipating mechanism while the flow passes through the orifice located in the middle of the horizontal column, four different orifice areas with area blocking ratios (Ψ) of 20%, 40%, 60% and 80%, respectively, are used in each configured group to calibrate the corresponding head loss coefficient η . The detail dimensions of each configured group are listed in Table 1; D represents the amplitude of the table displacement during harmonic forced vibration tests.

2.1 Calibration of the natural frequency

First, the four configured groups of the TLCs are sequentially placed on the shake table. The natural frequencies of the TLCs are calibrated for each group by recording the response of the free vibration tests, in which the liquid surface movement was excited by driving the shake table at a frequency close to the resonance frequency and then suddenly stopping its motion. Shown in the upper part of Table 2 are the natural frequencies thus measured for each group. It was found that the size of liquid mass does not have an effect on the natural frequency. The calibrated results in Table 2 concluded that the analytical natural frequency $\omega_d = (2g/L)^{1/2}/2\pi$ (Hz) is reliable because the errors between the measured and predicted frequencies are less than 2%.

2.2 Calibration of the head loss coefficient

To calibrate the head loss coefficient, the forced harmonic vibration tests are performed for each

Table 1 Dimensions of the configured groups of the TLCs

| | Model I | Model II | Model III | Model IV |
|--------------------------------|---------|----------|-----------|----------|
| L_h (cm) | 85 | 115 | 145 | 175 |
| L_v (cm) | 63.75 | 57.5 | 48.33 | 37.5 |
| $A_v = A_h$ (cm ²) | 15* 15 | 15* 15 | 15* 15 | 15* 15 |
| Blocking ratio(%) | 20,40 | 20,40 | 20,40 | 20,40 |
| | 60,80 | 60,80 | 60,80 | 60,80 |
| $p = L_h / L$ | 0.4 | 0.5 | 0.6 | 0.7 |
| L (cm) | 212.5 | 230 | 241.67 | 250 |
| D (cm) | 4 | 4 | 4 | 4 |

Table 2 Calibrated results of the TLC property tests

| | Configured group | | | |
|---|--------------------------------|--------------------------------|--------------------------------|--------------------------------|
| | I | II | III | IV |
| Natural frequency ω_d (rad/sec) (Error <i>w.r.t.</i> Predicted) | $0.4923 \times 2\pi$ (1.8%) | $0.4727 \times 2\pi$ (1.7%) | $0.4595 \times 2\pi$ (1.3%) | $0.4516 \times 2\pi$ (1.3%) |
| Head loss coefficient η | | | | |
| Blocking ratio $\Psi = 20\%$ | 3.96 | 3.55 | 3.40 | 3.40 |
| Blocking ratio $\Psi = 40\%$ | 6.10 | 5.80 | 5.70 | 5.55 |
| Blocking ratio $\Psi = 60\%$ | 12.80 | 12.40 | 12.50 | 12.00 |
| Blocking ratio $\Psi = 80\%$ | 54.50 | 54.00 | 59.00 | 56.00 |

group by driving the shake table at various frequencies, and hence the liquid response is recorded. The head loss coefficients are calibrated by comparing the measured amplitude responses of the liquid displacement and those from the analytical formula derived in the following. With ν being set to 1 and \hat{x} being substituted by $\frac{D}{L_h} e^{i2\pi kt}$, the response of \hat{y} can be easily solved in terms of k , $\varphi_{\hat{y}}$ and $e^{i2\pi kt}$. By taking the absolute value on both sides, the amplitude of \hat{y} can be solved as

$$\varphi_{\hat{y}} = \frac{\sqrt{-2\pi^2(1-k^2)^2 + (4\pi^4(1-k^2)^4 + k^8(8/3\eta p)^2 4\pi^2 \gamma^2)^{1/2}}}{k^2(8/3\eta p)} \quad (1)$$

$$p = L_h / L$$

$$k = \omega / \omega_d$$

$$\gamma = pD / L_h$$

$$\eta = (-0.6\Psi + 2.1\Psi^{0.1})^{1.6}(1-\Psi)^{-2}$$

$$L = 2L_v + L_h$$

ω : excitation frequency

ω_d : natural frequency of a TLCD;

Ψ : area blocking ratio in the orifice of a TLCD

η : head loss coefficient

For each configured group, by adjusting the head loss coefficient η to the proper values, the amplitude of \hat{y} versus k was plotted together with the experimental data to fit each other, as denoted by the solid curves shown in Fig. 3. The head loss coefficients thus calibrated is listed in

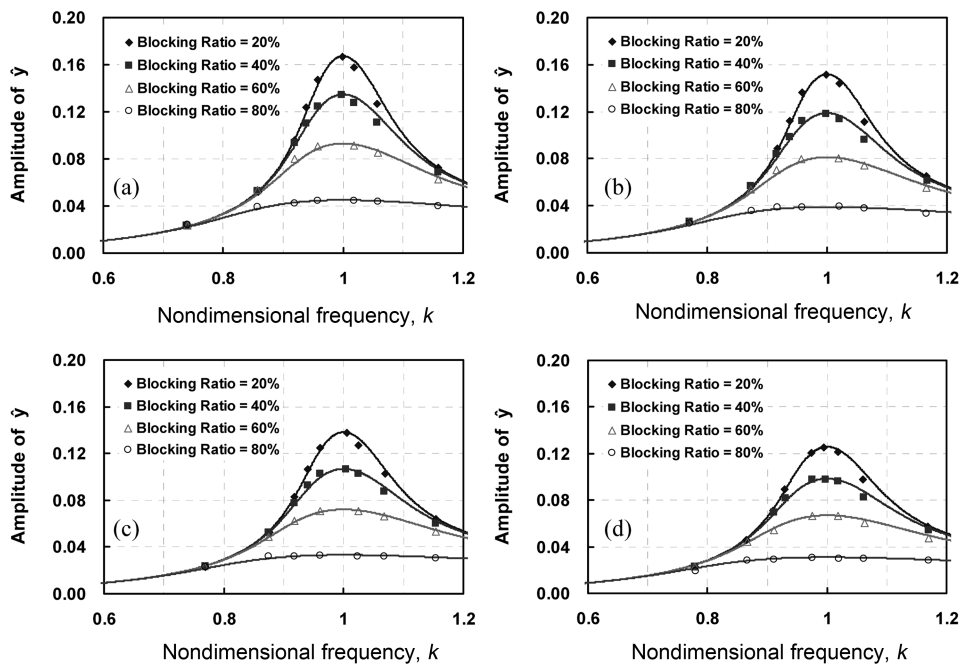


Fig. 3 Experimental results of \hat{y} amplitudes for each configured group of the TLCD in the forced vibration tests: (a) configured group I, (b) configured group II, (c) configured group III and (d) configured group IV

the lower part of Table 2. The detail information of the experimental calibration of the TLCD Properties can be obtained in the paper title of “Design guidelines for tuned liquid column damper for structures responding to wind” by Wu *et al.*(2005).

The meanings of the symbols are listed below:

- y : The amplitude of water (the largest amplitude under steady-state)
- \hat{y} : Dimensionless amplitude (the largest amplitude under steady-state)
- A_v : Cross-section area of the vertical post
- A_h : Cross-section area of the horizontal post
- L_h : Vertical length of post of the TLCD (Tuned liquid column damper)
- L_v : Horizontal length of post of the TLCD (Tuned liquid column damper)
- D : Amplitude of the harmonic motion on the vibration table

3. Numerical modeling and procedure

The numerical simulation tool used in this study was the computational fluid dynamics software, Fluent. Fluent is designed based on a finite volume discretization of the equations of motion. In this study, unsteady kappa-epsilon ($\kappa - \epsilon$) turbulence models with the VOF method and the sliding mesh technique are adopted to track the interface evolution of the water surface and also calculate the head loss coefficients and Natural frequency.

3.1 Mathematical model

The flow of water and air inside the TLCD is assumed to be an incompressible fluid with variable properties. RANS equations govern the fluid motion subject to the continuity constraint:

The Continuity Equation

$$\frac{\partial u_j}{\partial x_j} = 0 \quad (2)$$

The Momentum Equation

$$\frac{\partial u_i}{\partial t} + u_j \frac{\partial u_i}{\partial x_j} = -\frac{1}{\rho} \frac{\partial p}{\partial x_i} + \frac{\mu}{\rho} \frac{\partial^2 u_i}{\partial x_j \partial x_j} - \frac{\partial}{\partial x_j} (\overline{u_i' u_j'}) + g_i \quad (3)$$

$$-\overline{u_i' u_j'} = \frac{1}{\rho} \mu_t \left(\frac{\partial u_i}{\partial x_j} + \frac{\partial u_j}{\partial x_i} \right) - \frac{2}{3} k \delta_{ij} \quad (4)$$

Where, U is velocity, P is pressure, ρ is fluid density, $-\overline{u_i' u_j'}$ is Reynolds stress, g_i is gravity, and μ_t is eddy viscosities, respectively. The fluid properties are computed knowing the volume fraction of the liquid phase α_1 , introduced in the next section

$$\rho = \alpha_1 \rho_1 + (1 - \alpha_1) \rho_g \quad (5)$$

$$\mu = \alpha_1 \mu_1 + (1 - \alpha_1) \mu_g \quad (6)$$

where the subscripts l and g denote liquid and gas phase, respectively. A κ - ε model with a standard wall law is used for the turbulence. The turbulent kinetic energy, κ , and its dissipation rate ε , are obtained from

$$\frac{\partial \kappa}{\partial t} + u_j \frac{\partial \kappa}{\partial x_j} = \frac{1}{\rho} \frac{\partial}{\partial x_j} \left[\left(\mu + \frac{\mu_t}{\sigma_k} \right) \frac{\partial \kappa}{\partial x_j} \right] + \frac{G_k}{\rho} - \varepsilon \quad (7)$$

$$\frac{\partial \varepsilon}{\partial t} + u_j \frac{\partial \varepsilon}{\partial x_j} = \frac{1}{\rho} \frac{\partial}{\partial x_j} \left[\left(\mu + \frac{\mu_t}{\sigma_\varepsilon} \right) \frac{\partial \varepsilon}{\partial x_j} \right] + \frac{1}{\rho} C_{\varepsilon 1} G_k \frac{\varepsilon}{k} - C_{\varepsilon 2} \frac{\varepsilon^2}{k} \quad (8)$$

where C_μ , $C_{\varepsilon 1}$, $C_{\varepsilon 2}$, σ_k , and σ_ε are the default κ - ε model coefficients. $G_k = \mu_t S_i$ is the generation of turbulent kinetic energy due to mean velocity gradients with S_i the mean rate of strain tensor. The eddy viscosity is given by $\mu_t = C_\mu \rho \kappa^2 / \varepsilon$.

3.1.1 Free surface model

In CFD, the volume of fluid method (VOF) is a numerical technique for tracking and locating the free surface (or fluid-fluid interface). The VOF model can model two or more immiscible fluids by solving a single set of momentum equations and tracking the volume fraction of each of the fluids throughout the domain. The typical applications include the prediction of the jet breakup, the motion of the large bubbles in a liquid, the motion of liquid after a dam break, and the steady or transient tracking of any liquid-gas interface.

The VOF model relies on the fact that two or more fluids (or phases) are not interpenetrating. For each additional phase that adds to the model, a variable is introduced to the volume fraction of the phase in the computational cell. In each control volume, the volume fractions of all the phases sum to unity. The fields for all the variables and properties are shared by the phases and represent volume-averaged values, as long as the volume fraction of each of the phases is known at each location. Thus the variables and properties in any given cell are either purely representative of one of the phases, or representative of a mixture of the phases, depending upon the volume fraction values. In other words, if the q^{th} fluid's volume fraction in the cell is denoted as α_q , then the following three conditions are possible:

- $\alpha_q = 0$: The cell is empty (of the q^{th} fluid).
- $\alpha_q = 1$: The cell is full (of the q^{th} fluid).
- $0 < \alpha_q < 1$: The cell contains the interface between the q^{th} fluid and one or more other fluids.

Based on the local value of q^{th} , the appropriate properties and variables will be assigned to each control volume within the domain.

The Volume Fraction Equation

The tracking of the interface(s) between the phases is accomplished by the solution of a continuity equation for the volume fraction of one (or more) of the phases. For the q^{th} phase, this equation has the following form

$$\frac{\partial \alpha_q}{\partial t} + \mathbf{v} \cdot \nabla \alpha_q = \frac{S_{\alpha_q}}{\rho_q} \quad (8)$$

By default, the source term on the right-hand side of Eq. (8), S_{α_q} is zero, but a constant or user-defined mass source for each phase can be specified. The volume fraction equation will not be solved for the primary phase; the primary-phase volume fraction will be computed based on the

following constraint

$$\sum_{q=1}^n \alpha_q = 1 \quad (9)$$

3.1.2 Sliding mesh model

When a time-accurate solution for rotor-stator interaction is desired, the sliding mesh model is used to compute the unsteady flow field. The sliding mesh model is not only the most accurate method for simulating flows in multiple moving reference frames, but also the most computationally demanding. Most often, the unsteady solution that is sought in a sliding mesh simulation is time-periodic. That is, the unsteady solution repeats with a period related to the speeds of the moving domains. However, the other types of transients including translating sliding mesh zones can also be simulated. For example, two cars or trains pass in a tunnel.

The TLCD is a horizontal moving object, so the dynamic mesh model has to be used in the moving border. In this study, the moving behavior of the TLCD is a special case of the sliding mesh model. Usually there is a virtual (grid) interface between rotor and stator at sliding mesh model. However, there is no interface set in the case because TLCD model moved the whole calculation domain. The walls of TLCD and the internal grids move simultaneously, so the grid is not reorganized or deformed.

3.2 Numerical model

In this study, the multiphase flow model that includes air and water is selected. By using the sliding mesh and the dynamic mesh technique of the Fluent, the TLCD is able to achieve the simple harmonic motion in horizontal. Moreover, by using the VOF model, we can further track the location of the water surface after being vibrated. However, in the case of free surface simulation, the influence of the gravity field needs to be considered. That is, the gravity is set to be 9.81m/s^2 . Fig. 4 shows the structure grid and refined grid at the region of the free surface at the calculation domain.

In order to obtain the optimum parameters, which include the selections of turbulence model,

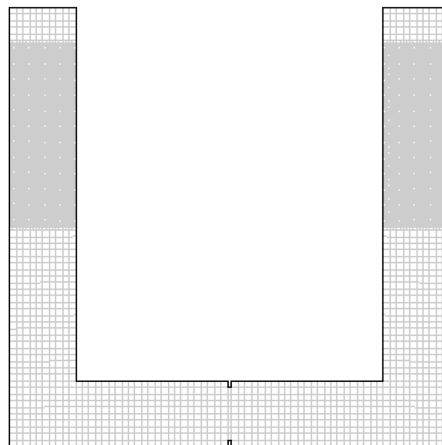


Fig. 4 The structure grid and refined grid at region of free surface

boundary condition, simulation time duration, time step size, and grid size etc., the different combination of parameter cases are tested. Fig. 5 showed the numerical domain and the settings of boundary condition. Table 3 lists the parameter settings of final numerical model. Fig. 6 shows the

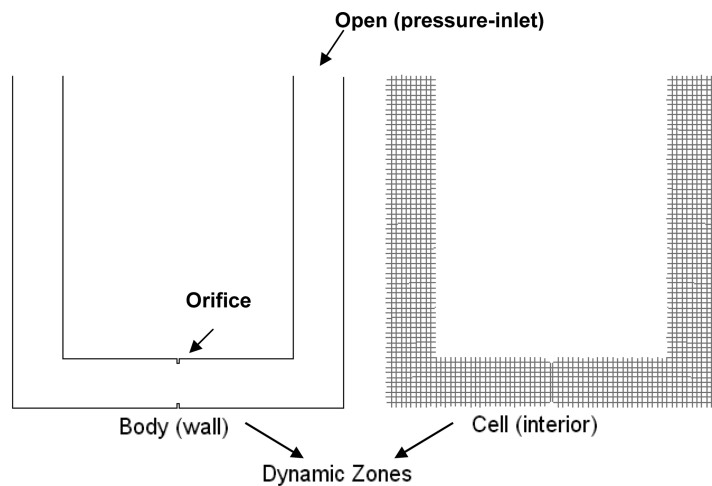


Fig. 5 Numerical domain and settings of the boundary condition

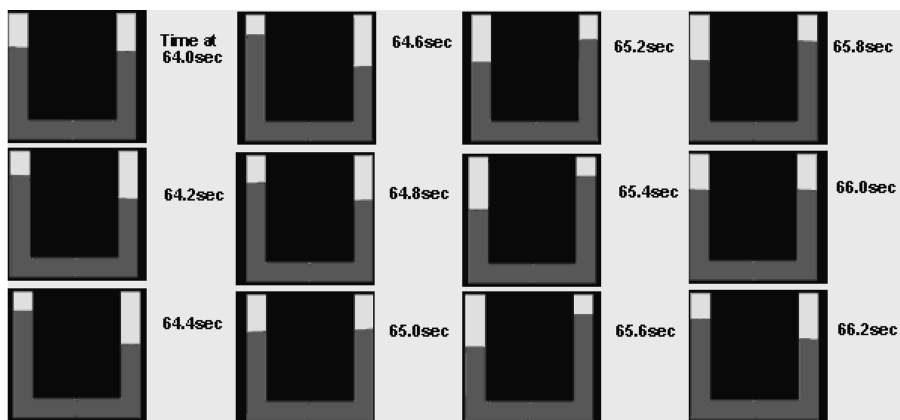


Fig. 6 Continuous pictures of the moving amplitude of water in the TLCD for time duration from 64 sec to 66.2 sec

Table 3 Numerical solution parameters used in the CFD simulation

| | |
|-----------------------------|--|
| Numerical model | Unsteady time-depend Standard κ - ε model and VOF model |
| Computational domain | Same with the experiments (table 1) |
| Boundary conditions | Sliding mesh and dynamic mesh model |
| Computational grid | Structured grid and refined grid at region of free surface |
| Simulation time duration | 80 seconds |
| time step size | 0.01 second |
| Under-relaxation parameters | VOF: 0.4 (pressure), 0.7 (velocity) |

change of the dimensionless amplitude of water inside the vertical columns of the TLCD of configured group I that is in red (dark) color for simulation time duration between 64 seconds and 66 seconds. The turbulent flow model is a standard $k-\varepsilon$ model with the blocking ratio of 20%, and the vibration frequency is 0.49167 per sec.

4. Comparison of the simulation results to the experimental results

The comparison of the dimensionless amplitude of the CFD and the experiment are shown in Fig. 7. Overall, the CFD prediction of the configured group I represents the best among other three models. If the blocking ratio is considered in the case, the bigger the blocking ratio, the better the accuracy of the CFD predictions. For example, the configured group III represents the worst CFD predictions if considering the locking ratios. When the blocking ratio is 20%, the prediction difference between the CFD and the experiment is around 10%. If the blocking ratio is 80%, the prediction difference is around 3%. When the blocking ratio is 0%, the CFD prediction for dimensionless amplitude is relatively close to the prediction of dimensionless amplitude when the blocking ratio is 20%. (The experiment does not perform with the blocking ratio 0%). If the nondimensional frequency is considered, when the excitation frequency is equal to the natural frequency, the prediction difference between the CFD and the experiment is the greatest. If the nondimensional frequency is either lower

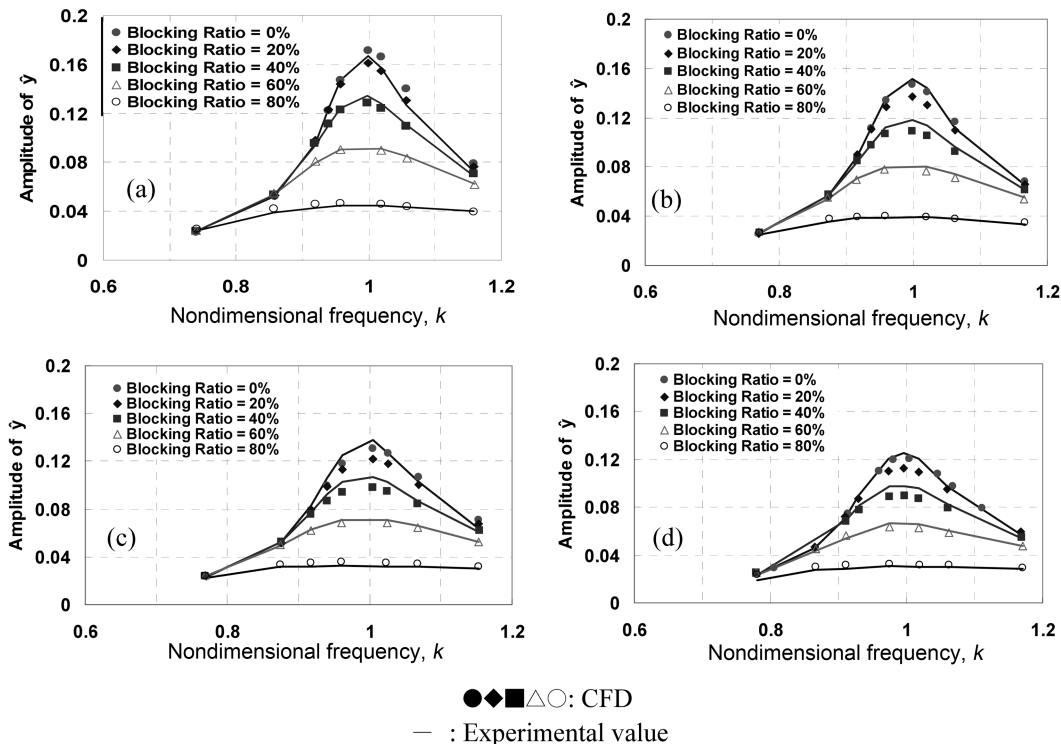


Fig. 7 Comparisons of amplitudes with experiment and CFD in forced vibration tests: (a)configured group I, (b)configured group II, (c)configured group III and (d)configured group IV

Table 4 Comparisons of head loss coefficient with experiment and CFD

| Head loss coefficient | Experiment | CFD | Experiment | CFD | Experiment | CFD | Experiment | CFD |
|------------------------------|------------|-------|------------|-------|------------|-------|------------|------|
| | I | | II | | III | | IV | |
| Blocking ratio $\Psi = 0\%$ | - | 3.74 | - | 3.74 | - | 3.77 | - | 3.66 |
| Blocking ratio $\Psi = 20\%$ | 3.96 | 4.25 | 3.55 | 4.29 | 3.4 | 4.3 | 3.4 | 4.25 |
| Blocking ratio $\Psi = 40\%$ | 6.1 | 6.56 | 5.8 | 6.67 | 5.7 | 6.68 | 5.55 | 6.69 |
| Blocking ratio $\Psi = 60\%$ | 12.8 | 12.99 | 12.4 | 13.07 | 12.5 | 13.22 | 12 | 13.4 |
| Blocking ratio $\Psi = 80\%$ | 54.5 | 51.2 | 54 | 51.15 | 59 | 51.01 | 56 | 51.2 |

Table 5 Natural frequency of experiment and CFD as compared with theory

| Analytical natural frequency | | I | II | III | IV |
|------------------------------|---------------------------------|----------------------|----------------------|----------------------|----------------------|
| | $w_d = (2g / L)^{1/2}$ (rad/s) | | $0.4836 \times 2\pi$ | $0.4648 \times 2\pi$ | $0.4535 \times 2\pi$ |
| Experiment | Natural frequency w_d (rad/s) | $0.4923 \times 2\pi$ | $0.4727 \times 2\pi$ | $0.4595 \times 2\pi$ | $0.4516 \times 2\pi$ |
| | (Error <i>w.r.t</i> predicted) | 1.8% | 1.7% | 1.3% | 1.3% |
| CFD | Natural frequency w_d (rad/s) | $0.4909 \times 2\pi$ | $0.4713 \times 2\pi$ | $0.463 \times 2\pi$ | $0.4542 \times 2\pi$ |
| | (Error <i>w.r.t</i> predicted) | 1.5% | 1.4% | 2.1% | 1.9% |

or higher, the CFD has more accurate predictions.

The process of obtaining the head loss coefficient and the natural frequency by using the numerical simulation results is the same as using the experimental data. The head loss coefficients calibrated by using the CFD data are compared with the head loss coefficients calibrated by using the experimental data. As shown in Table 4, the head loss coefficients obtaining from both the CFD predictions and the experiment are very close. It is also noted that for each blocking ratio, the CFD predicts relatively close head loss coefficient values for each configured groups. Therefore, it can be concluded that the head loss coefficient is neither affected by the different size of liquid mass nor by the different configurations (different ρ). It is only significantly affected by the area blocking ratio Ψ in the orifice. Table 5 shows the natural frequencies of both the experiment and the CFD compared with the analytical natural frequencies with blocking ratio 20% for four configured groups. The difference of the TLCD natural frequency calibrated by the CFD and analytical natural frequency is about 1% to 2%. Similarly, the difference of the TLCD natural frequency calibrated by the experiment and analytical natural frequency is about 1% to 2%.

5. Conclusions

It is concluded that the CFD software, Fluent, can effectively predict the free surface of water inside the vertical columns of the TLCD, and calibrate the natural frequencies of the TLCD with different moving frequencies and blocking ratios by combining both the volume of fluid (VOF) method and the sliding mesh technique. The results of the comparison between the numerical simulations and the experimental measurements show that it is not difficult to achieve similar trends in flow behavior inside the TLCDs if the adequate grid resolution, accurate boundary conditions and improved turbulence models are provided. The study concludes that the CFD is relatively reliable in

the research and development of TLCD.

Acknowledgements

The work upon which this paper is based was supported by a grant from the National Science Council (NSC 95-2221-E-032-054-MY3). The valuable experimental data from Prof. Jong-Cheng Wu at the Department of Civil Engineering and Wind Engineering Research Center of Tamkang University is gratefully acknowledged.

References

- Balendra, T., Wang, C.M. and Rakesh, G. (1998), "Effectiveness of TLCD on various structural systems", *Eng. Struct.*, **21**(4), 291-305.
- Chang, C.C. (1999), "Mass dampers and their optimal designs for building vibration control", *Eng. Struct.*, **21**(5), 454-463.
- Chen, Q., Dai, G.Q., Zhu, F.Q. and Yang, Q. (2004), "Three-dimensional Turbulence numerical simulation of a tepped spillway overflow", *J. Hydrodynamics.*, **16**(1), 74-79.
- Chen, Z., Kurokawa, Y. and Nishimoto, H. (2006), "CFD application on the development of circulating water channel", *Proceedings of the International Offshore and Polar Engineering Conference*, San Francisco, California, USA, May.
- Chuan Fu (2009), "Passive vibration control of plan-asymmetric buildings using tuned liquid column gas dampers", *Struct. Eng. Mech.*, **33**(3).
- De Souza, S.L.T., Caldas, I.L., Viana, R.L., Balthazar, J.M. and Brasil, R.M.L.R.F. (2006), "Dynamics of vibrating systems with tuned liquid column dampers and limited power supply", *J. Sound Vib.*, **289**(4-5), 987-998.
- Felix, J.L., Balthazar, P.J.M. and Brasil, R.M.L.R.F. (2005), "On tuned liquid column dampers mounted on a structural frame under a non-ideal excitation", *J. Sound Vib.*, **282**(3-5), 1285-1292.
- Filippone, A. (2005), *Simulation of rotating cylinder with sliding meshes*, 43rd AIAA Aerospace Sciences Meeting and Exhibit-Meeting Paper, 11299-11308.
- Hirt, C.W. and Nichols, B.D. (1981) "Volume of fluid (VOF) method for the dynamics of free boundaries", *J. Comput. Phys.*, **39**(1), 201-225.
- Hitchcock, P.A., Kwok, K.C.S. and Watkins, R.D. (1997), "Characteristics of Liquid Column Vibration Absorbers (LCVA) – II", *Eng. Struct.*, **19**(2), 135-144.
- Liovic, P., Liow, J. L. and Rudam, M. (2001), "A volume of fluid method for simulation of metallurgical flows", *ISIJ International.*, **41**(3), 225-233.
- Maronnier, V., Picasso, M. and Rappaz, J. (2003), "Numerical simulation of three-dimensional free surface flows", *Int. J. Numer. Meth. Fl.*, **42**(7), 697-716.
- Martinez-Calle, J., Gonzalez-Perez, J., Balbona-Calvo, L. and Blanco-Marigorta, E. (2002), "An open water numerical model for a marine propeller: a comparison with experimental data", American Society of Mechanical Engineers, Fluids Engineering Division (Publication) FED., **257**(2B), 807-814.
- Min, K.W., Kim, H.S., Lee, S.H., Kim, H. and Ahn, K. (2005), "Performance evaluation of tuned liquid column dampers for response control of a 76-story benchmark building", *Eng. Struct.*, **27**(7) 1101-1112.
- Sakai, F., Takaeda, S. and Tamaki, T. (1989), "Tuned liquid column damper-new type device for suppression of building vibration", *Proceedings of the International Conference on High-rise Building*, Nanjing, China.
- Wu, J.C., Wang, Y.P., Lee, C.L., Liao P.H. and Chen, Y.H. (2008), "Wind-induced interaction of a non-uniform tuned liquid column damper and a structure in pitching motion", *Eng. Struct.*, **30**(12), 3555-3565.
- Wu, J.C., Shih, M.H. Lin, Y.Y. and Shen, Y.C. (2005), "Design guidelines for tuned liquid column damper for structures responding to wind", *Eng. Struct.*, **27**(13), 1893-1905.

- Xu, Y.L., Samali, B. and Kwok, K.C.S. (1992), "Control of along-wind response of structures by mass and liquid dampers", *J. Eng. Mech.-ASCE*, **118**(1), 20-39.
- Xue, S.D., Ko, J.M. and Xu, Y.L. (2000), "Tuned liquid column damper for suppressing pitching motion of structures", *Eng. Struct.*, **23**(11) 1538-1551.
- Yalla, S. and Kareem, A. (2000), "Optimum absorber parameters for tuned liquid column dampers", *J. Struct. Eng.-ASCE*, **126**(8), 906-915.
- Chen, Y.H. and Ding, Y.J. (2008), "Passive, semi-active, and active tuned-liquid-column dampers", *Struct. Eng. Mech.*, **30**(1), 99-106.
- Zhou, J., Yu, W. and Zhou, C. (2008), "Numerical study on mixing process of immiscible polymer melts in internal batch mixer using two-dimensional model", *J. Polym. Eng.*, **28**(6-7), 385-404.
- "FLUENT 6.2 Users Guide", <http://www.fluent.com>
- "Gambit 2.2 Users Guide", <http://www.fluent.com>

CC